PERGAMON

International Journal of Multiphase Flow 25 (1999) 15–33

International Journal of Multiphase Flow

A computational study of the inertial lift on a sphere in a linear shear flow field

P. Cherukat [a,*], J.B. McLaughlin [a], D.S. Dandy [b]

[a] Department of Chemical Engineering, Clarkson University, Potsdam, NY, 13699-5705, USA
[b] Chemical and Bioresource Engineering Department, Colorado State University, Fort Collins, CO, 80523, USA

Received 13 February 1997; received in revised form 20 May 1998

Abstract

The shear induced inertial migration of a rigid sphere has been studies computationally by simulating the flow around a rigid sphere with a Fourier finite volume technique. The values of the lift force obtained by flow simulation have been compared with those predicted by asymptotic analyses for rotating and non-rotating spheres. © 1999 Elsevier Science Ltd. All rights reserved.

Keywords: Inertia; Lift; Shear

1. Introduction

A rigid sphere that translates in a linear shear flow field will experience a lift force. Using reversibility arguments, it can be shown that the creeping flow equations do not predict any lift force. The lift force arises from inertial effects. Saffman (1965, 1968) derived an asymptotic expression for the lift force by singular perturbation techniques. Saffman assumed that $\sqrt{Re_G} \gg Re_s$ (where Re_G is the sphere Reynolds number based on the velocity gradient and Re_s is the sphere Reynolds number based on the slip velocity). In other words, the initial terms due to the shear are large compared to the inertial terms due to the slip velocity of the sphere.

Asmolov (1989) and, independently, McLaughlin (1991) generalized Saffman's analysis to allow for the possibility that $\sqrt{Re_G} \sim Re_s$ Their expression for the lift force reduces to Saffman's expression when $\sqrt{Re_G}/Re_s \to \infty$. When $\sqrt{Re_G} \sim Re_s$ the lift force is smaller than that predicted by Saffman's analysis and when $\sqrt{Re_G}/Re_s \to 0$ the lift force is very small and changes sign. Saffman's analysis and its generalization are based on singular perturbation

* Corresponding author. Tel. 001 617 949 1764; Fax: 001 617 949 1030; E-mail: pradeep.cherukat@aspentech.com

PII: S0301-9322(98)00034-2

techniques. In these analyses, the failure of regular perturbation expansions is due to the existence of an outer region in the flow field. In Saffman's analysis, the outer flow field is at a distance that is $O(\sqrt{v/G})$. The lift force arises due to the transverse component of the disturbance flow in the outer region. In Asmolov and McLaughlin's analyses, the outer region is at a distance that is $\min[O(\sqrt{v/G}), O(v/V_s)]$. In all cases, it was assumed that all the Reynolds numbers are small compared to unity.

Another related problem is the lift on a sphere translating and spinning in a quiescent fluid. Rubinow and Keller (1961) did an asymptotic analysis of this problem and derived an expression for the lift force. Saffman (1965) also obtained an expression for the second order correction to the lift. This correction has two terms; the first one is identical to the Rubinow–Keller expression and the second one is formally of the same order but of opposite sign.

Auton (1987) analyzed the lift on a sphere translating in weak shear flow of an inviscid fluid and obtained an expression for the lift force. This expression is valid when the change in incident velocity of the undisturbed flow field across the sphere is much smaller than the slip velocity of the sphere.

In this paper we will describe a numerical study of the inertial lift on a sphere in a linear shear flow for Reynolds numbers that are $O(1)$. This numerical study has been conducted for both stationary spheres and freely rotating spheres. The motivation for the study was the observation that the lift force can be important in determining the trajectory of particles and drops in a turbulent flow near a solid wall (McLaughlin, 1989). In such situations the Reynolds numbers are typically $O(1)$ and it is required to ascertain whether the asymptotic expression can be used without any serious errors. Dandy and Dwyer (1990) conducted a numerical study of the lift and drag on a stationary sphere in a linear shear flow field. Most of the data reported by these authors were for high Reynolds numbers. Their data for Reynolds numbers that are $O(1)$ indicated good agreement with Saffman's (1965) analysis. Mei (1992) obtained an expression for the lift force that is valid for all Reynolds numbers by fitting an equation to Dandy and Dwyer's (1990) data for high Reynolds numbers and Saffman's expression for low Reynolds numbers.

Several authors have reported experimental data on inertial lift (Segré and Silberberg, 1961; Goldsmith and Mason, 1967; Cox and Mason, 1971) Most of the data is for flow of suspensions in tubes and channels and is related to tubular pinch formation. Cherukat, et al. (1994) conducted an experimental study of lift in a linear shear flow field. They measured the inertial migration velocity of spheres sedimenting in a linear shear flow field. A linear shear field was produced using a homogeneous shear flow apparatus in which two rubber timing belts moved in opposite directions. They found that the experimentally measured migration velocities agree with those obtained using the asymptotic expression derived by McLaughlin (1991). In the above experiments, wall effects were not important. The effect of a rigid wall has been considered by a number of workers in the field. Asymptotic analyses have been done for situations for which the outer region flow does not contribute to the lift force to leading order (Cox and Brenner, 1968; Cox and Hsu, 1977; Ho and Leal, 1976; Leighton and Acrivos, 1985; Cherukat and McLaughlin, 1993) and also for cases in which the flow in the outer region affects the lift force to leading order (Drew, 1988; Schonberg and Hinch, 1989; McLaughlin, 1993).

The main contribution of this paper is the set of results for the lift force on a sphere when the particle Reynolds number is $O(1)$. Most existing results for the lift force are based on asymptotic expansions in the Reynolds numbers. Previous numerical work concentrated mainly on Reynolds numbers that are large compared to unity. The few existing experimental measurements in linear shear flows are of the migration velocity. The relationship between the migration velocity and the lift force in a shear flow is not clear a-priori when the Reynolds numbers are not small compared to unity. It will be seen that previously published asymptotic results provide reasonable estimates for the lift force provided that the shear rate is sufficiently strong.

2. Numerical study of the lift force

Consider a rigid sphere of radius a in a linear shear flow field as shown in Fig. 1. The fluid is assumed to be Newtonian with a kinematic viscosity v, dynamic viscosity μ and density ρ. Consider a Cartesian coordinate system (x, y, z) and a spherical polar coordinate system (r, θ, ϕ) as shown in Fig. 1. The unit vectors in the x, y and z directions are $\mathbf{e}_x$, $\mathbf{e}_y$ and $\mathbf{e}_z$. In the absence of the sphere, the undisturbed flow field is given by $Gx\mathbf{e}_z$. The sphere moves with a velocity $-V_s\mathbf{e}_z$ relative to the undisturbed flow field. In a reference frame that moves with the sphere, the velocity of the undisturbed flow is $(Gx + V_s)\mathbf{e}_z$. Consider a computational domain Γ that consists of the space between the rigid sphere and an imaginary concentric spherical surface at a sufficiently large distance from the sphere. The Navier–Stokes equations and the continuity equation can be integrated over an arbitrary volume Ω and expressed as

$$Re\iiint_{\Omega}\frac{\partial \mathbf{u}^*}{\partial t}\mathrm{d}V + Re\iiint_{\Omega}(\mathbf{u}^*\cdot\nabla\mathbf{u}^*)\mathrm{d}V = -\iint_{\partial\Omega}P^*\cdot\mathbf{n}\mathrm{d}S + \iint_{\partial\Omega}\mathbf{n}\cdot\tau\mathrm{d}S, \tag{1}$$

$$\iint_{\partial\Omega}\mathbf{n}\cdot\mathbf{u}^*\mathrm{d}S = 0, \tag{2}$$

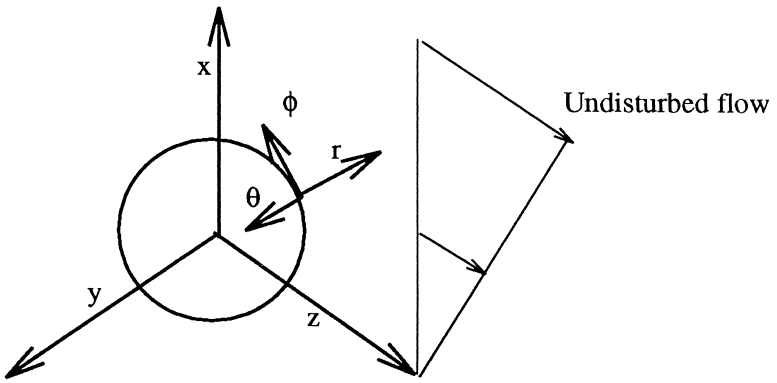

Fig. 1. The coordinate system for simulation of a uniform shear flow around a sphere.

along with the boundary conditions

$$\mathbf{u}^* = \mathbf{u}^*_{\mathrm{b}} \text{ on } \partial\Gamma, \tag{3}$$

where $\partial\Omega$ and $\partial\Gamma$ denote the boundaries of Ω and Γ respectively, $\mathbf{u}^*$ is the dimensionless velocity obtained by dividing the velocity by the slip velocity of the sphere, τ is the dimensionless viscous stress, P^* is the dimensionless pressure, Re is the Reynolds number based on the slip velocity and the radius of the sphere and $\mathbf{n}$ is the unit vector normal to $\partial\Omega$. If the force on the sphere is $\mathbf{F}$, then the dimensionless force $\mathbf{F}^*$ is defined by

$$\mathbf{F}^* = \frac{\mathbf{F}}{\mu a V_{\mathrm{s}}}. \tag{4}$$

In general, the force on the sphere will have non-zero components in the x direction (lift) and the z direction (drag):

$$\mathbf{F}^* = F^*_{\mathrm{lift}}\mathbf{e}_x + F^*_{\mathrm{drag}}\mathbf{e}_z. \tag{5}$$

A finite set of points called nodes are generated in the computational domain and the computational domain is then divided into discrete non-overlapping cells (see Fig. 2). One applies (1) and (2) to these cells to derive the finite volume equations. A detailed discussion of the generation of nodes and cells and the derivation of various forms of finite volume equations may be found in Anderson et al. (1984) and Vinokur (1989). In this study, a grid of

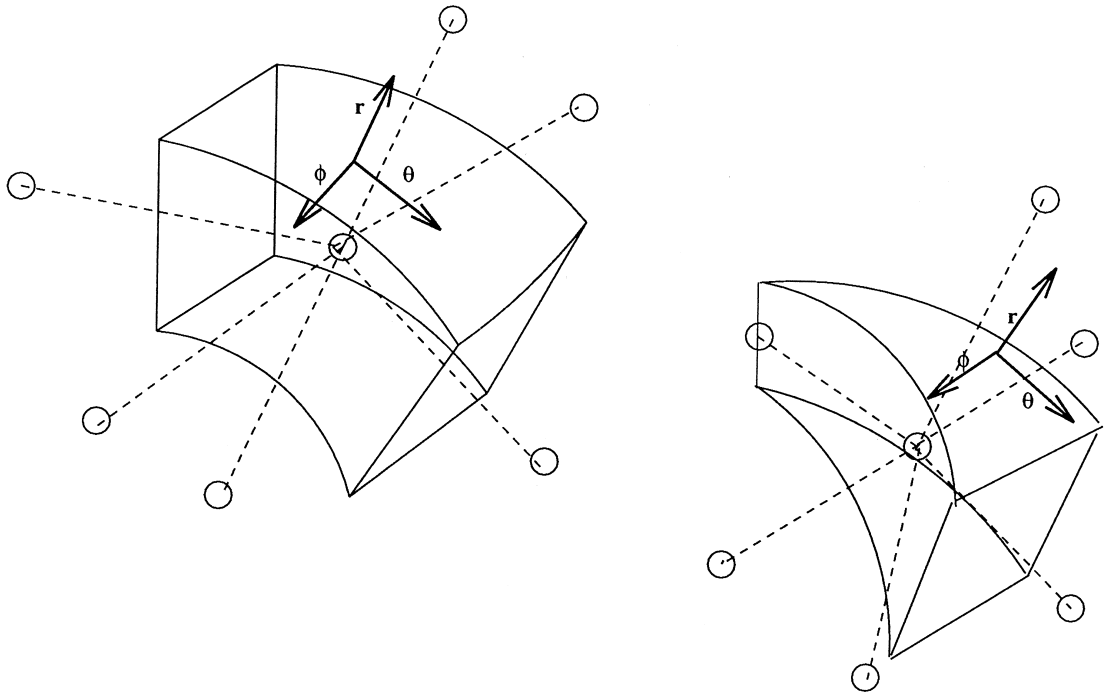

Fig. 2. Six and five faced cells used for discretizing the domain.

nodes that conform to a spherical coordinate system was generated. Each node lies entirely within a cell. The cells can have six faces or five faces (see Fig. 2), and each cell has one node in its interior. The five faced cells occur near the poles $\theta = 0$ and $\theta = \pi$. Each node is identified by an ordered integer triplet. The cell surrounding the node (l, m, n) is called the cell (l, m, n). The θ and ϕ coordinates of the node (l, m, n) are given by

$$\theta_m = \frac{m\pi}{N_\theta - 1} m = 0, \ldots, N_\theta - 1, \tag{6}$$

$$\phi_l = \frac{2\pi l}{N_\phi} l = 0, \ldots, N_\phi - 1, \tag{7}$$

where N_θ is the number of nodes in the θ direction and N_ϕ is the number of nodes in the ϕ direction. The nodes in the radial direction are chosen to lie on the surface of spheres concentric with the body. For flows past rigid surfaces, the variations in the flow field are largest near the surface of the body. Hence, a non-uniform spacing of the nodes in the radial direction was chosen. The value of r corresponding to the nth node in the radial direction is the Chebyshev collocation point given by

$$r_n = 1 + \left[1 - \cos\left(\frac{n\pi}{2(N_r - 1)}\right)\right](R_\mathrm{o} - 1) n = 0, \ldots N_r - 1, \tag{8}$$

where N_r is the number of nodes in the radial direction and R_o is the radius of the outer boundary. The nodes generated using (8) are densely packed near the surface of the sphere. This distribution of the nodes in the r direction was chosen based on the results obtained for Stokes flows. It was found that the computed values of the drag force were closer to that obtained using the analytical expression when the grid stretching (8) was used as compared with an algebraic grid stretching. The boundary, $\partial\Omega_{lmn}$ of the cell (l, m, n) is the union of the cell faces.

The surface and volume integrals in (1) and (2) must be expressed in terms of the values of the field variables at the nodes. The resulting system of algebraic equations is solved numerically. Several methods may be used for expressing the surface integrals in (1) and (2) in terms of the values of the variables at the nodes. The most commonly used method is to approximate the variables at cell faces by interpolating linearly between adjacent nodes. Dandy and Dwyer (1990) used this method in their study of inertial lift on a rigid sphere. The advantages of this method are that the resulting algebraic system is sparse and the generation of the coefficients of the algebraic system of equations is computationally inexpensive. However, a large number of nodes is required to obtain accurate results for the spatial variation of the field variables. Since the geometry of the problem is spherical, the velocity and pressure fields are periodic in the azimuthal coordinate, ϕ, when r and θ are fixed. Hence, they may be expressed as Fourier series in F:

$$\mathbf{u}^*(\phi, \theta, r) = \sum_{q=-N_\phi/2}^{N_\phi/2-1} \tilde{\mathbf{u}}_\mathrm{q}(\theta, r) e^{iq\phi}, \tag{9}$$

$$P^*(\phi, \theta, r) = \sum_{q=-N_\phi/2}^{N_\phi/2-1} \tilde{P}_q(\theta, r) e^{iq\phi}. \tag{10}$$

The Fourier coefficients in (9) and (10) are given by

$$\tilde{\mathbf{u}}_m(\theta, r) = \frac{1}{N_\phi} \sum_{j=0}^{N_\phi-1} \mathbf{u}^*(\phi_j, \theta, r) e^{-im\phi_j}, m = -N_\phi/2, \ldots, N_\phi/2 - 1, \tag{11}$$

and

$$\tilde{P}_m(\theta, r) = \frac{1}{N_\phi} \sum_{j=0}^{N_\phi-1} P^*(\phi_j, \theta, r) e^{-im\phi_j}, m = -N_\phi/2, \ldots, N_\phi/2 - 1, \tag{12}$$

where

$$\phi_j = \frac{2\pi j}{N_\phi}, j = 0, \ldots, N_\phi - 1. \tag{13}$$

To obtain the values of the velocity and the pressure on the r and the θ faces, it is assumed that these quantities vary linearly between the nodes straddling these faces. Using (9)–(12), the surface integrals and volume integrals in (1) and (2) may be evaluated.

Eqs. (1) and (2) are applied to each cell in the computational domain for the x, y and z components of the velocity. Thus, the discrete approximation of the finite volume equations expressed in terms of the Cartesian components of the velocity field using a grid that conforms to a spherical polar coordinate system is

$$\mathbf{M}\frac{\mathrm{d}\bar{\mathbf{u}}}{\mathrm{d}t} + \mathbf{N}(\bar{\mathbf{u}})\bar{\mathbf{u}} = -\mathbf{D}\bar{P} + \mathbf{A}\bar{\mathbf{u}}, \tag{14}$$

$$\mathbf{C}\bar{\mathbf{u}} = 0, \tag{15}$$

where $\bar{\mathbf{u}}$ and $\bar{\mathbf{P}}$ are the vectors containing velocities and pressures at the nodes. $\mathbf{A}\bar{\mathbf{u}}$ gives the surface integral of the viscous stress, $\mathbf{D}\bar{P}$ gives the surface integral of pressure, and $\mathbf{C}\bar{\mathbf{u}}$ gives the mass flux over the surface of each cell in the computational domain. $\mathbf{N}\bar{\mathbf{u}}$ gives the volume integral of the convective acceleration term and $\mathbf{M}(\mathrm{d}\bar{\mathbf{u}}/\mathrm{d}t)$ gives the volume integral of the temporal derivative term over the cell. Eqs. (14) and (15) form a system of $4N_\phi N_\theta N_r$ non-linear equations. The linear terms $\mathbf{M}(\mathrm{d}\bar{\mathbf{u}}/\mathrm{d}t)$, $\mathbf{A}\bar{\mathbf{u}}$ and $\mathbf{D}\bar{P}$ and $\mathbf{C}\bar{\mathbf{u}}$ were evaluated by expressing the velocity and pressure fields as Fourier expansions in ϕ (9) and (10), and then expressing the Fourier coefficients of the velocity and pressure fields in terms of the variables at the nodes using (11) and (12). The integration over the cell faces was done analytically, using linear interpolation in the θ and r directions. Thus, the discrete approximation of all the linear terms in the finite volume equations for all the cells can be expressed as a product of a matrix and a vector of the velocities and pressures at the nodes. The matrices **M**, **A**, **C** and **D** depend only on the grid. A detailed derivation of these matrices can be found in Cherukat (1993).

The time dependent Eq. (14) and (15) were advanced in time by a first order implicit Euler time stepping scheme. We did not use a higher order time stepping scheme since we were not interested in the transients. To avoid solving a system of non-liner equations, the non-linear term was expressed as $\mathbf{N}(\bar{\mathbf{u}}^k)\bar{\mathbf{u}}^{k+1}$, where the superscript denotes the time step. The term $\mathbf{N}(\bar{\mathbf{u}}^k)\bar{\mathbf{u}}^{k+1}$ is the discrete approximation of the volume integral $\iiint_\Omega(\mathbf{u}^*\cdot\nabla\mathbf{u}^*)$ in (1), and was evaluated in the following manner: the velocity fields at the kth and $(k+1)^{\text{st}}$ time steps were expressed in terms of these velocity fields at the nodes in the ϕ direction using (9) and (11). The integrations in the r, θ and ϕ directions for each cell were done analytically. This results in an expression of the form $\mathbf{N}(\bar{\mathbf{u}}^k)\bar{\mathbf{u}}^{k+1}$. Since the time stepping was done on the variables in the physical space, there was no need to de-alias the computations.

To obtain the field at time step $k+1$ the following system of algebraic equations was solved:

$$\begin{bmatrix} (-\mathbf{A}+\mathbf{N}(\bar{\mathbf{u}}^k)+\frac{1}{\Delta t}\mathbf{M}) & \mathbf{D} \\ \mathbf{C} & \mathbf{H} \end{bmatrix} \begin{bmatrix} \bar{\mathbf{u}}^{k+1} \\ \bar{P}^{k+1} \end{bmatrix} = \begin{bmatrix} \frac{1}{\Delta t}\mathbf{M}\mathbf{u}^k \\ 0 \end{bmatrix}. \tag{16}$$

$\mathbf{H}$ is a $(N_r N_\theta N_\phi)\times(n_r N_\theta N_\phi)$ matrix. The calculations were started from an initial state and the time stepping was done until a steady state solution was reached. We were interested in the transient behavior of the solutions. The time step was chosen such that the problem did not diverge. Also, since the simulations that we did were for low Reynolds numbers, the high viscosity might have damped most of the instabilities associated with the time stepping.

The pressure does not appear in the continuity equation for incompressible flows. Also, there are no boundary conditions on the pressure. Hence, the elements of $\mathbf{H}$ are zero. However, the pressure can be determined only up to an arbitrary constant in incompressible flows. To remove this hydrostatic indeterminacy, Dirichlet boundary conditions are imposed on the pressure at certain nodes in the domain. The disturbance pressure on the nodes on the outer boundary of the computational domain was set to zero. The continuity equations for the cells next to the outer boundary were removed from the system of equations. This gives a square system of equations with non-zero elements in $\mathbf{H}$ along the diagonal. The matrices $\mathbf{A}$, $\mathbf{D}$, $\mathbf{C}$, and $\mathbf{M}$ are time independent and are generated in a preprocessor step. The matrix $\mathbf{N}$, however, has to be generated at each time step. If $\mathbf{N}$ and $\mathbf{M}$ are zero, then (16) is the discrete approximation to the steady state creeping flow equations. This linear system may be solved to obtain the steady state creeping flow solution. For obtaining the steady state solution of the full Navier–Stokes equations, the creeping flow solution was used as the initial condition. The velocity boundary conditions were substituted for the momentum balance equation at those nodes where velocity boundary conditions were specified.

The linear system (16) is very large and sparse. For the simulations described in this paper, 8 nodes were used in the ϕ direction, 40 nodes were used in the θ direction and 65 nodes were used in the r direction and the linear system consists of 83,200 equations. Iterative methods are frequently used to solve linear algebraic systems of equations. Kyrlov subspace methods are a terminating class of algorithms; i.e. for non-singular coefficient matrices, it may be shown that these methods converge to the solution in a finite number of steps (see Golub and Van Loan, 1989). In the GMRES method (Saad and Schultz, 1986), the solution is approximated by a linear combination of the orthonormal basis vectors of an expanding Krylov subspace. The

computations involved are, essentially, the evaluation of inner products. These computations are very fast on the IBM RISC 6000 processors on which we performed all our simulations. The coefficient matrix need not be generated fully and stored for performing these computations. The main drawback of the GMRES method is that the number of iterations required for finding a solution depends on the condition number of the coefficient matrix. The memory requirements and the number of floating point operations increases with the number of iterations, since each iteration generates a new vector in the orthonormal basis set for the Krylov subspace. Since the system of Eq. (16) is generally ill-conditioned, the restarted version, GMRES(m), was used. In this method, after m iterations the GMRES method is restarted with the solution obtained after m iterations as the starting value. The system (16) is the discrete approximation to a differential algebraic system (DAE). The continuity equation is a purely algebraic constraint to the momentum balance equation. When differential algebraic systems are approximated by backward difference formulas like the implicit Euler method, the coefficient matrix in (16) becomes ill conditioned as the step size decreases (see Petzold and Lötstedt, 1986). The values of the velocity and pressure fields obtained in the previous time step were used as the initial guess for starting the GMRES algorithm.

The boundary conditions depend on the nature of the boundaries. No-slip boundary conditions are applied on the surface of the sphere. Since the flow is an unbounded shear flow, the disturbance flow on the outer boundary will be zero if the outer boundary is sufficiently far from the surface of the sphere. In most of the simulations described in this paper, the outer boundary was located at 75 sphere radii from the center of the sphere and zero disturbance flow was assumed on the outer boundary. The drag force obtained for the Stokes problem is shown as a function of the location of the outer boundary in Fig. 3. It was found that, for Stokes flow problems with the domain truncated at 75 radii, the computed drag force is within 3% of the exact analytical solution. A very large computational domain will be required to obtain a numerical solution which is exactly equal to the analytical solution. In (16), the momentum equations on the boundary nodes are replaced by the boundary conditions and the resulting system of linear algebraic equations is solved to compute the velocity and pressure at each time step.

For a freely rotating sphere, the instantaneous dimensionless torque, T^*, can be related to the angular acceleration by the expression

$$T^* = M_I \frac{d\omega}{dt}, \tag{17}$$

where M_I is the moment of inertia of the sphere. The torque balance Eq. (17) was used to update the angular velocity. At each time step, the velocity and pressure fields were computed keeping the value of ω fixed. The torque on the sphere was computed based on the computed velocity and pressure fields and the angular velocity was updated by a first-order explicit scheme:

$$\omega^{*k+1} = \omega^{*k} + \frac{T^*}{M_I}\Delta t, \tag{18}$$

where ω^* is the angular velocity at the kth time step. The transient response of a freely rotating sphere depends on the value of M_I. However, the steady state solution is independent

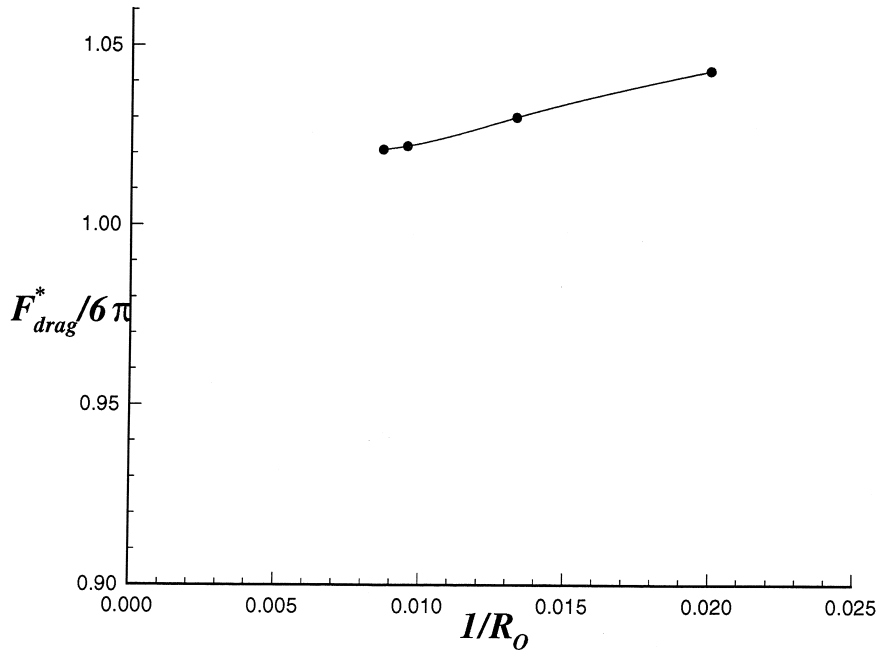

Fig. 3. The variation of the computed value of the lift force with the size of the computational domain for Stokes flow.

of the value of M_I. In these computations, the steady state solutions were studied and the value of M_I was chosen to make the explicit time stepping scheme stable. At steady state, the torque acting on the sphere is zero.

3. Analysis of the lift obtained by numerical simulation of the flow field

For the flow described in Section 2, the Reynolds number based on the velocity gradient may be defined as

$$Re_G = \frac{4Ga^2}{v}, \tag{19}$$

and the Reynolds number based on the slip velocity may be defined as

$$Re_s = \frac{2aV_s}{v} \tag{20}$$

Flow simulations were done for $Re_G = 0.04$, 0.06, 0.08 and 0.10 for values of Re_s in the range 0.02–2.0. The simulations were done for stationary and rotating spheres. As mentioned in Section 2, the computations were done with the outer boundary located at 75 radii from the center of the sphere. This domain truncation has an effect on the computed values of the lift

and drag forces. Masliyah and Epstein (1970) have shown by perturbation analysis that locating the outer boundary at 100 radii for axisymmetric creeping flow past a sphere over-predicts the drag coefficient by about 2%. The effect of truncation of the outer boundary has a larger influence on the lift force than on the drag force since the lift is due to the inertial effects at large distances from the sphere. This was also observed by Dandy and Dwyer (1990) in their computational study of inertial lift on a sphere. The lift force is several times smaller than the drag force, and the effect of boundary truncation and numerical errors are likely to cause a larger relative error in the lift than on the drag.

When Re_G, $Re_s \ll 1$, to leading order, the equation of motion in the other region may be expressed as

$$(V_s + Gx)\frac{\partial \mathbf{v}_d}{\partial z} + G\mathbf{v}_d \cdot \mathbf{e}_x = -\frac{1}{\rho}\nabla p + \nu\nabla^2\mathbf{v}_d - 6\pi a\nu V_s \mathbf{e}_z \delta(\mathbf{r}), \tag{21}$$

where $\mathbf{v}_d$ is the disturbance flow and $\delta(\mathbf{r})$ is the three dimensional Dirac delta function. The assumption that Saffman made about the relative magnitudes of the Reynolds numbers may be stated in terms of length scales as

$$\left|\frac{\nu}{V_s}\right| \gg \sqrt{\frac{\nu}{G}}, \tag{22}$$

The above condition implies that the inertial effects due to shear are large compared to the inertial effects due to the slip velocity, and to leading order, the equation of motion in the outer region reduces to

$$Gx\frac{\partial \mathbf{v}_d}{\partial z} + G\mathbf{v}_d \cdot \mathbf{e}_x = -\frac{1}{\rho}\nabla p + \nu\nabla^2\mathbf{v}_d - 6\pi a\nu V_s \mathbf{e}_z \delta(\mathbf{r}). \tag{23}$$

Thus, Saffman's analysis applies to a sphere moving slowing in a strong shear field. Saffman's expression for the dimensionless lift force, F^*_{lift}, is

$$F^*_{\text{lift}} = 3.23 Re_G^{1/2}. \tag{24}$$

McLaughlin (1991) generalized Saffman's analysis by removing the restriction (22) and derived an expression for the inertial lift force by solving (21). The parameter ϵ was defined as

$$\epsilon = \frac{\sqrt{Re_G}}{Re_s}. \tag{25}$$

His result for the dimensionless lift force is

$$F^*_{\text{lift}} = 3.23 Re_G^{1/2}\left(\frac{\mathbf{J}(\epsilon)}{2.255}\right). \tag{26}$$

The function $\mathbf{J}$ is a three dimensional integral that depends only on the magnitude of ϵ. The function $\mathbf{J}$ has a value 2.255 as $\epsilon \to \infty$ (the Saffman limit), and as the value of ϵ decreases, $\mathbf{J}$ decreases rapidly. Saffman's analysis also gives the second order correction to the lift force. This second order correction is $O(Re_G)$ and the outer flow field does not contribute any terms

of this order to the second order correction. The expression for the lift force when the second order correction is also considered is

$$F^*_{\text{lift}} = 3.23\sqrt{Re_{\text{G}}}\frac{\mathbf{J}(\epsilon)}{2.255} - \frac{11\pi}{32}Re_{\text{G}}, \tag{27}$$

for a non-rotating sphere. The dimensionless lift force, F^*_{lift}, obtained by flow simulation has been plotted as a function of Re_{s} for several values of Re_{G} in Fig. 4. Each of these sets of data was obtained by keeping the value of Re_{G} fixed and varying in the slip velocity. It can be seen that F^*_{lift} does not change with Re_{s} when Re_{s} is very small. The range of values of Re_{s} for which the lift force F^*_{lift} is approximately a constant, corresponds to large values of ϵ, and this behavior of F^*_{lift} agrees with that predicted by (27). The value of the lift force for $\epsilon > 5$ has been plotted as a function of $Re_{\text{G}}^{1/2}$ in Fig. 5. The lift force predicted by Saffman's leading order expression (24) and that predicted by the second order formula (27) has also been plotted in Fig. 5. For $\epsilon > 5$, the computed values of the lift force agree with those predicted by (27) to within 6%. This discrepancy is mainly due to the truncation of the domain. As mentioned before, the simulations were done using an outer boundary that was 75 radii from the center of the sphere. A few simulations were done with a domain that was 105 radii. The values of the lift force obtained from these large domain simulations have been compared with

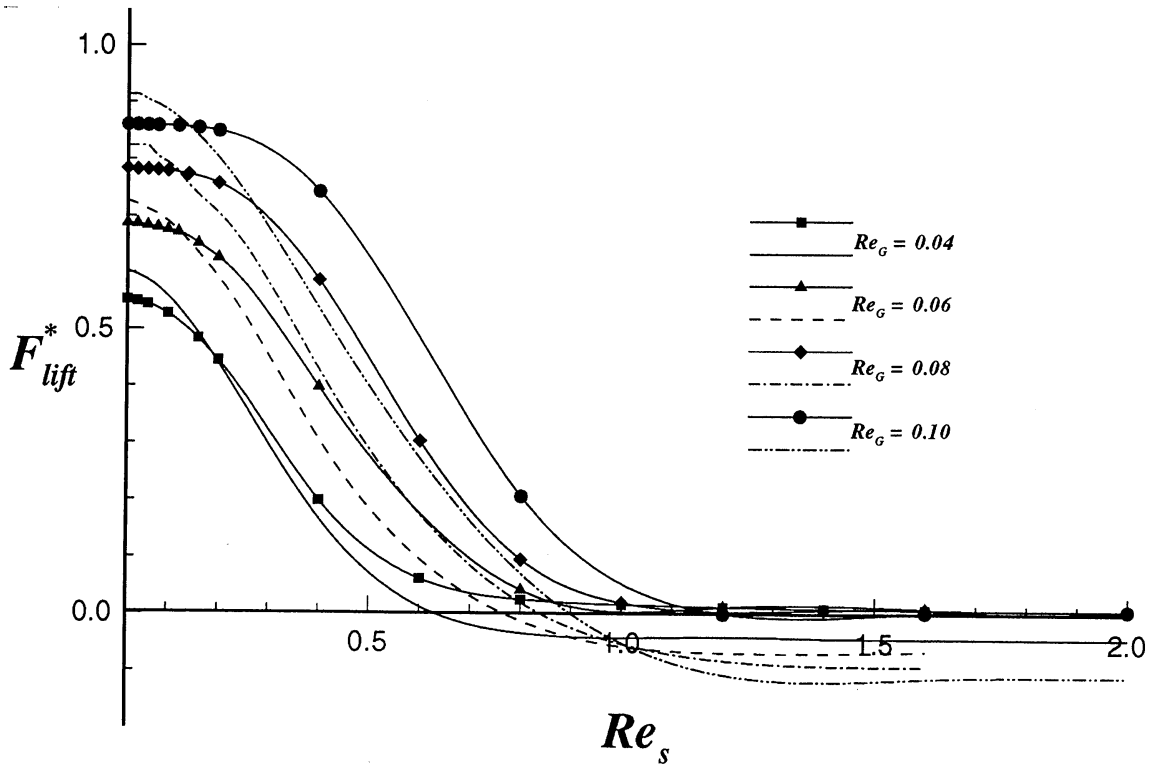

Fig. 4. Dimensionless lift force F^*_{lift} on a non-rotating sphere as a function of Re_{s} for $Re_{\text{G}} = 0.04$, 0.06, 0.08 and 0.10. The lines without the symbols represent the lift force obtained using (27).

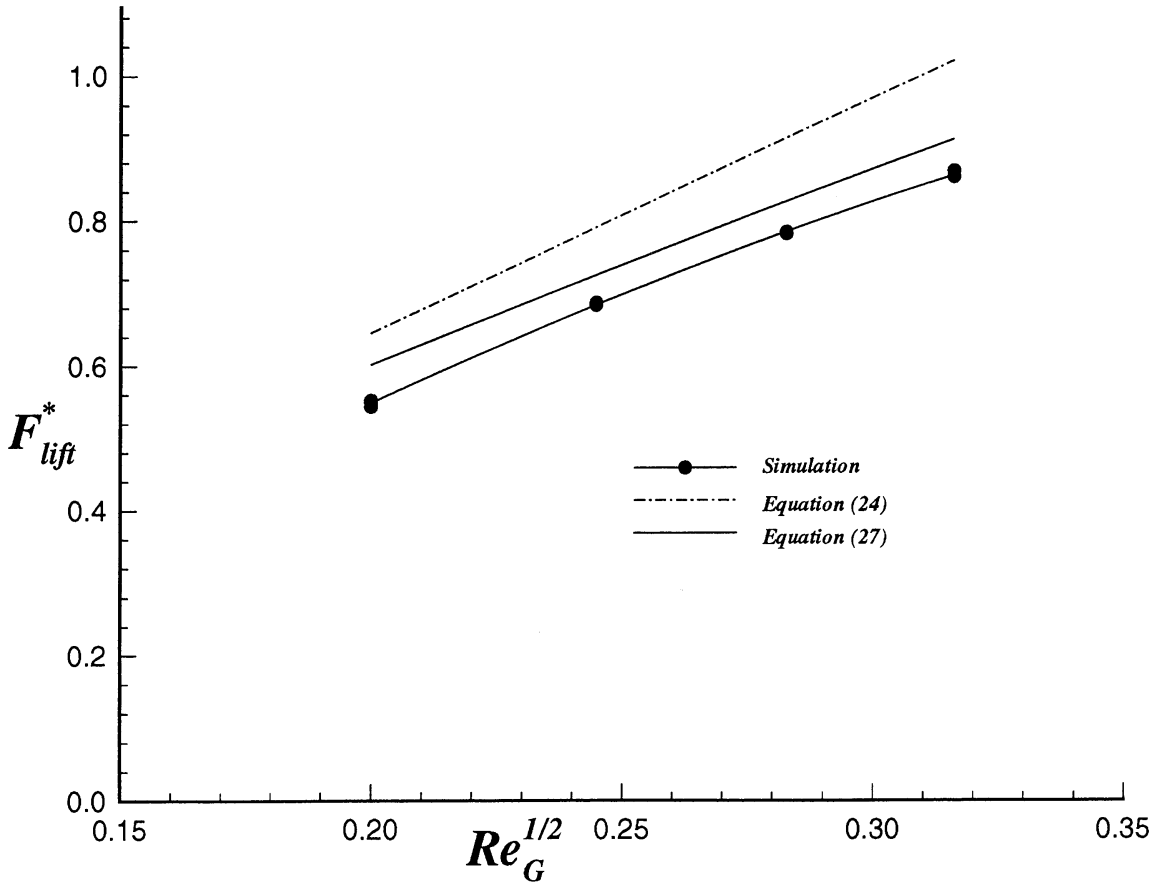

Fig. 5. Variation of the dimensionless lift force F^*_{lift} with $\sqrt{Re_G}$ for values of $\epsilon > 5.0$.

those obtained with the outer boundary located at 75 radii from the center of the sphere in Fig. 6. In these runs, $Re_G = 0.04$. It can be seen that the values of the lift force obtained by the large domain simulations are larger than those obtained by the corresponding simulations using the smaller domain. Thus, the truncation of the domain has an effect on the computed values of the lift and the dependence of the computed value of the lift force on the size of the computational domain for $Re_G = 0.04$ and $Re_s = 0.02$ is shown in Fig. 7. For the large domain simulations (with the outer boundary at 105 radii), the number of equations in the linear system that had to be solved at each time step was 102,400. The computational requirements for these simulations (the number of floating point operations and the memory requirements) are very large, mainly due to the larger number of iterations the GMRES algorithm requires for convergence. Hence, we could not conduct simulations with larger domains.

For each value of Re_G, as Re_s increases, F^*_{lift} decreases as predicted by (27). According to (27), the first order term in this equation decreases as Re_s increases since ϵ decreases as Re_s increases for a fixed value of Re_G. The second order term is a negative constant. Hence, for values of Re_s that are large ($Re_s \gg \sqrt{Re_G}$ to be precise), the asymptotic theory predicts that the lift force should be negative and the dominant contribution should be due to the second order

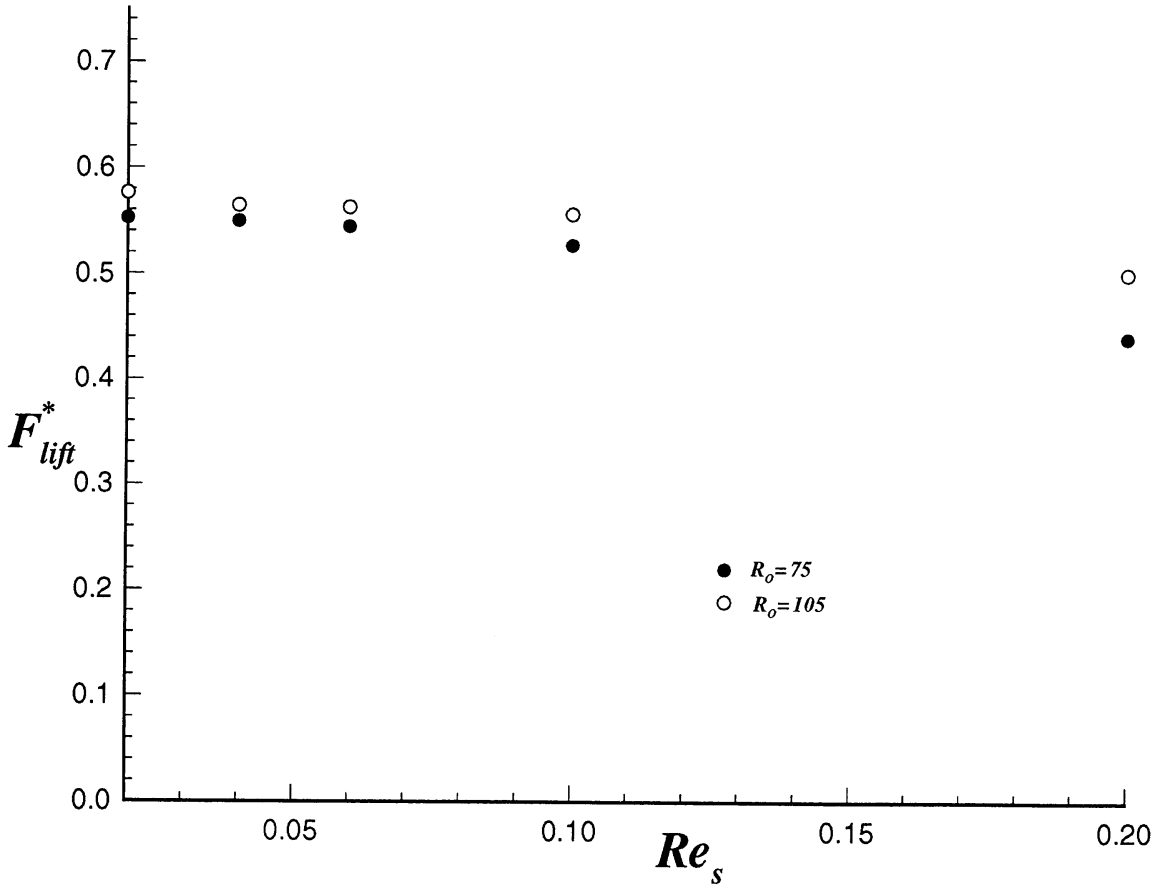

Fig. 6. The lift force obtained with simulations in which the outer boundary was located at 105 radii from the sphere and those in which the outer boundary was located at 75 radii from the sphere for $Re_G = 0.04$.

term. However, our computations do not indicate any change in direction of the lift force for values of Re_s that are large compared to $\sqrt{Re_G}$. The smallest value of ϵ that was considered in this study was 0.10, and the lift force even for this small value of ϵ was found to be positive. Though the truncation of the domain has an effect on the computed values of the lift force, when Re_s is large than $\sqrt{Re_G}$, the lift is caused by inertial effects that become important at distances that are $O(v/V_s)$. Hence, for values of Re_s that are an order of unity or larger, the effect of domain truncation is likely to be small as compared to those cases in which Re_s is very small. The leading order term in (27) is obtained by solving (21) for the flow in the outer region. The terms that are linear in the disturbance velocity have been retained in (21). This assumption is valid provided that the terms that are quadratic in the disturbance velocity are smaller than the terms that have been retained in (21). This will be true only if Re_s satisfies the inequality $Re_s \ll \epsilon^2$. This inequality imposes a very stringent condition on the slip Reynolds number when ϵ is small. In our simulations, when ϵ is small, Re_s does not satisfy the required inequality. This may explain the discrepancy in the values of the lift force obtained by flow simulation and those obtained using (27) when $Re_s \gg \epsilon$.

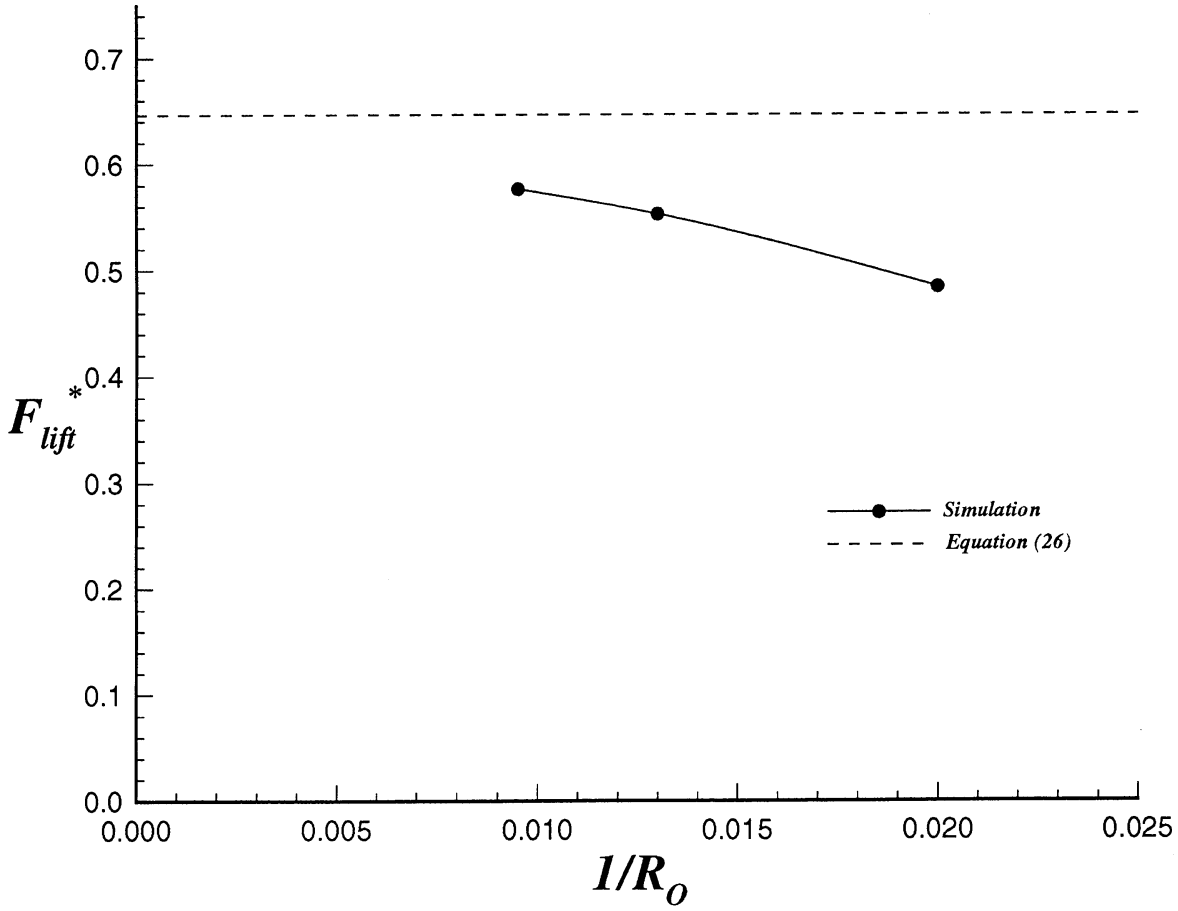

Fig. 7. The computed value of the lift force as a function of the size of the computational domain for $Re_G = 0.04$, $Re_s = 0.02$.

The lift force is obtained by integrating the pressure stress and the viscous stress over the surface of the sphere. The contribution of the pressure and the viscous stress to the lift force has been plotted in Fig. 8. Our computations indicate that, when Re_s is small, the viscous part of the lift force is very nearly equal to twice the pressure part of the lift force. This is in agreement with the leading order asymptotic analyses which show that, to leading order, the lift force arises due to the x component of the disturbance flow in the outer region. This flow appears to the sphere as a uniform flow in the x direction and the lift force is given by the drag produced by this disturbance flow. Thus, the lift force, to lowest order, is given by the Stokes drag due to the x-component of the disturbance flow at the location of the particle, which is a mathematical point in terms of a coordinate scaled by an appropriate length scale. As Re_s increases, initially, the viscous and pressure parts of the lift force decrease with the viscous part decreasing twice as fast as the pressure part. Subsequently, the viscous part continues to decrease and the pressure part appears to attain a constant value. The value of Re_s at which this happens depends on the value of Re_G. For values of Re_s that are larger than

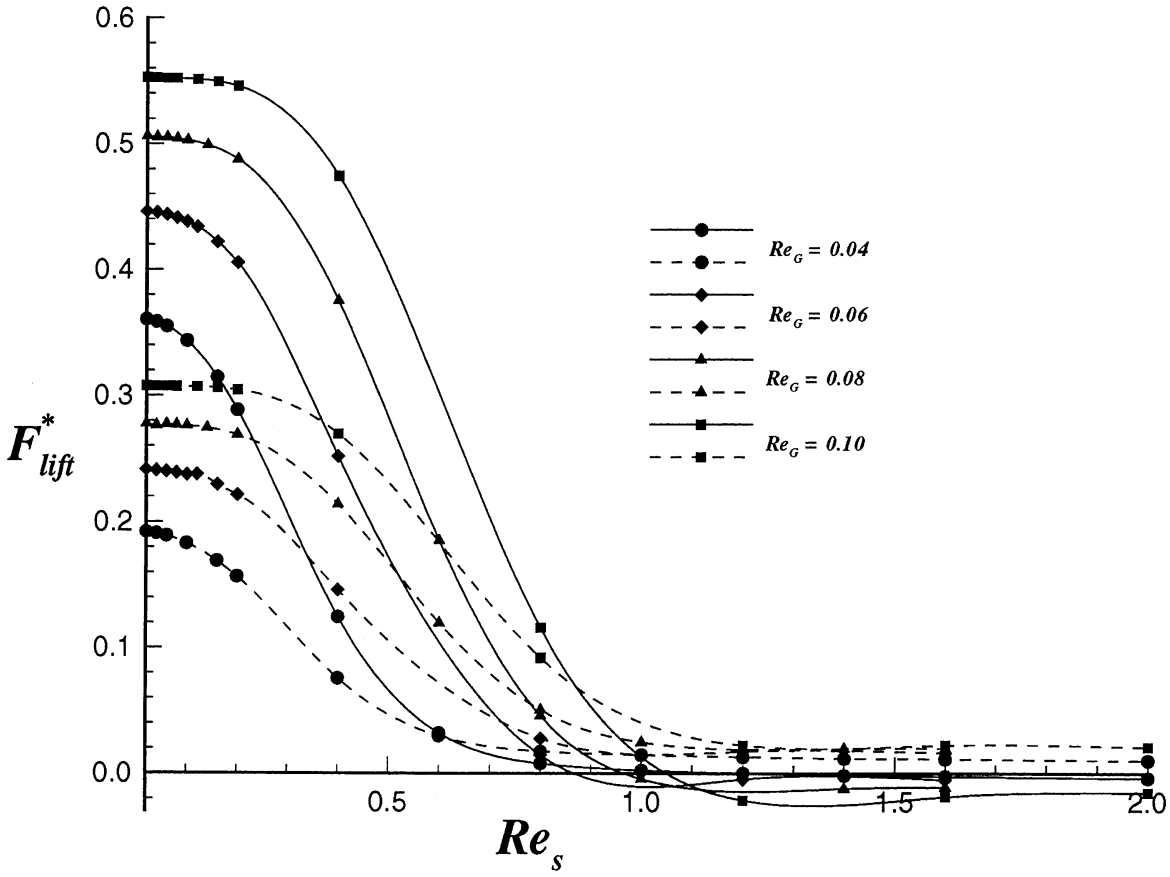

Fig. 8. The contributions from the pressure and viscous stresses to the lift force for a non-rotating sphere. The solid lines indicate the viscous contribution and the broken lines indicate the pressure contribution.

1.0, the viscous part is very small and shows very small negative values. The pressure part of the lift force is a constant and the dominant contribution to the lift force is due to the pressure.

When the sphere is free to rotate, the torque balance equations were solved in each time step. At steady state, the torque on a freely rotating sphere is zero. It was observed that the angular velocity of the sphere is equal to half the local vorticity when the slip Reynolds number is close to zero. As the slip Reynolds number increases, the angular velocity decreases. The ratio of the angular velocity of the sphere to the angular velocity obtained by solving the Stokes equations is shown in Fig. 9. In this figure, Re_G was in the range 0.04–0.10. When Re_s is equal to 1, the angular velocity of the sphere is about 94% of the value obtained by solving the Stokes equations.

The lift force on rotating and non-rotating spheres have been compared in Fig. 10. The effect of rotation is to produce an additional lift in the direction of the computed lift on a stationary sphere. When Re_s is small (i.e., large values of ϵ), the increase in the lift force is very small compared to the total lift force. According to Saffman's analysis, the lift on a rotating

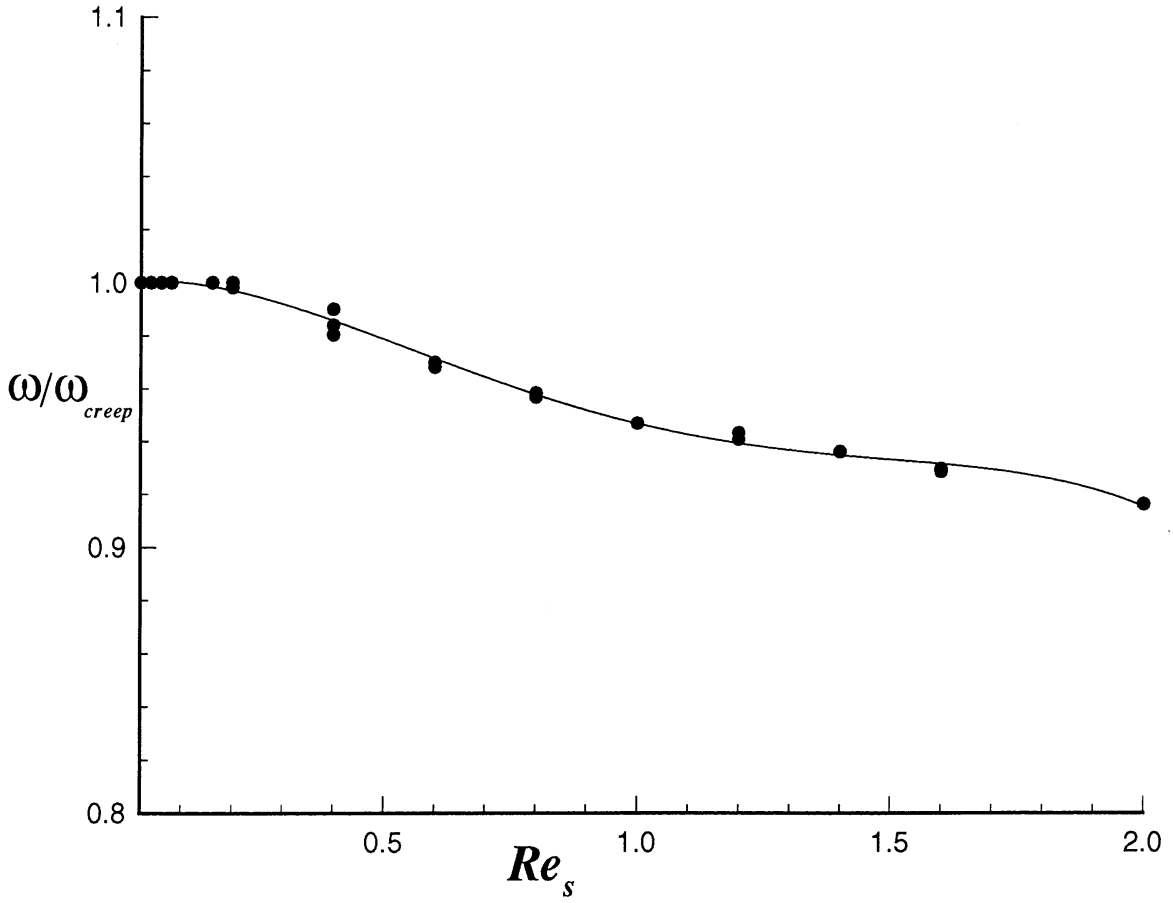

Fig. 9. The ratio of angular velocity of a sphere to the angular velocity under creeping flow conditions as a function of Re_s.

sphere is

$$F^*_{\text{lift}} = 3.23\sqrt{Re_G}\,\frac{\mathbf{J}(\epsilon)}{2.255} - \frac{11\pi}{32}Re_G + \frac{\pi}{4}Re_\Omega, \tag{28}$$

where Re_Ω is the Reynolds number based on the diameter of the sphere and angular velocity. The last term on the right hand side of (28) is equal to the expression that was obtained by Rubinow and Keller (1961) for the lift on a sphere translating and rotating in a quiescent fluid. For values of Re_s that are large (i.e. when ϵ is small), the lift on a non-rotating sphere is very small and the increase in the lift force due to the rotation of the sphere is comparable to the total lift force. The difference between the lift force on a rotating sphere and the lift force on a non-rotating sphere has been plotted as a function of Re_s for several values of Re_G in Fig. 11. This has been compared with the value given by Saffman's analysis. The increase in the lift force due to the rotation agrees with that given by Saffman's analysis to within 8% when Re_s

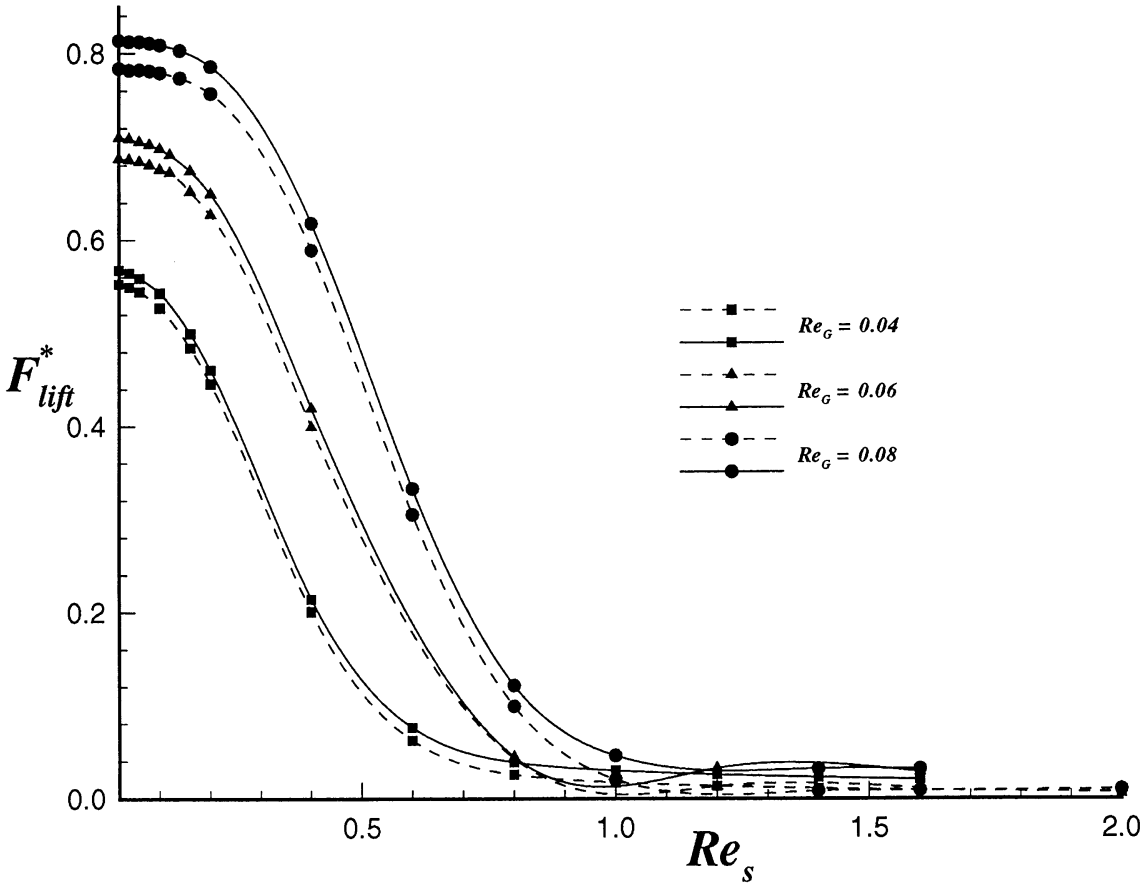

Fig. 10. Dimensionless lift force, F^*_{lift} on non-rotating and rotating spheres as a function of Re_s. The solid lines represent the lift on rotating spheres and the broken lines indicate the lift on stationary spheres.

is smaller than 0.5. For Re_s close to 1.0, the difference in the values obtained by flow simulation and those obtained using the asymptotic expressions (27) and (28) are larger.

4. Conclusion

This computational study indicates that the lift force obtained using (27) and (28) is reasonably accurate when the slip Reynolds numbers are $O(1)$. The computed values and those predicted by the asymptotic theories do not match perfectly. However, the qualitative behavior of the lift force obtained by flow simulations and using the asymptotic expressions are similar. Both the computed values and the asymptotic theories show that the lift force decreases rapidly when $Re_G^{1/2}$ becomes smaller then Re_s. The computed values not indicate any change in the direction of the lift force when $Re_s \gg \sqrt{Re_G}$. Part of the discrepancy between the values obtained by flow simulation and those obtained using the asymptotic expression could be explained by the effect of the domain truncation. This is likely to be large when the slip Reynolds number is

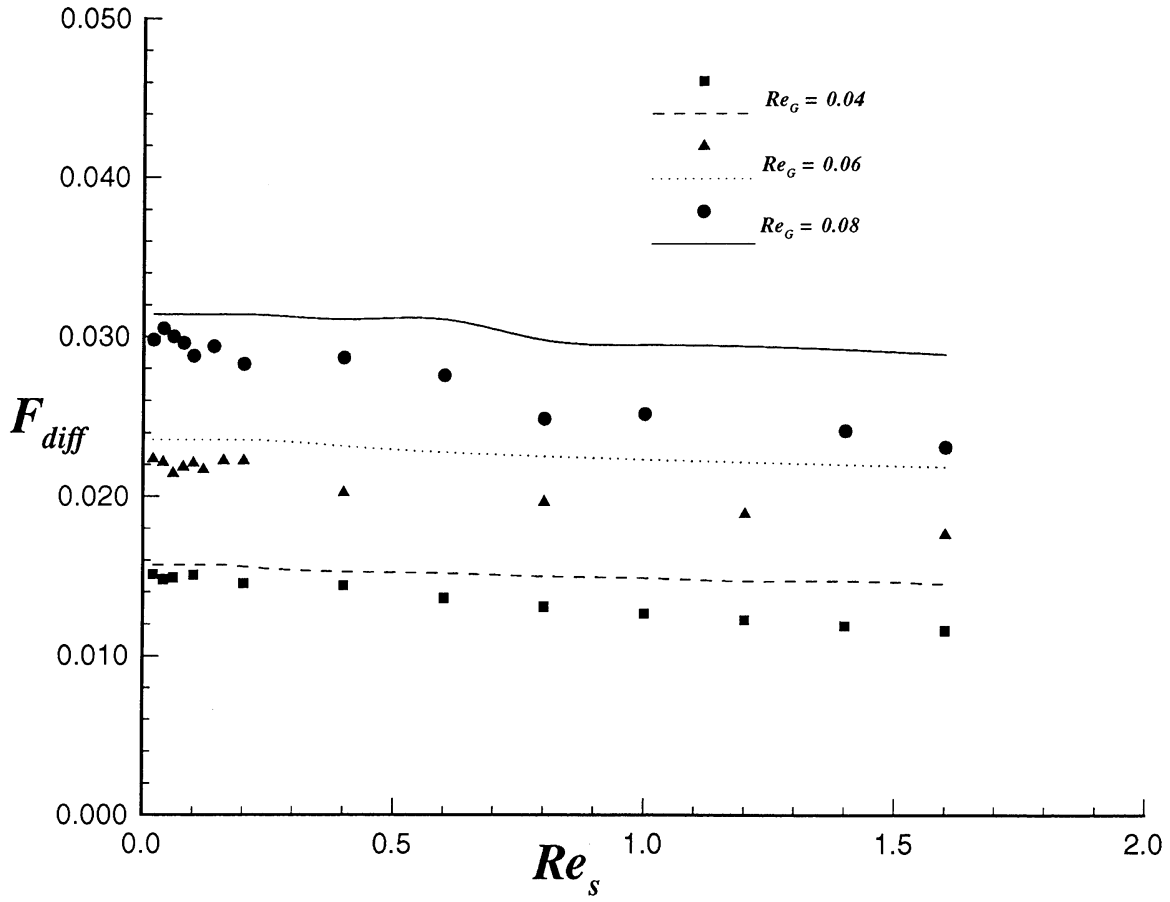

Fig. 11. The difference F_{diff} in the lift force on rotating spheres and non-rotating spheres. The curves represent the difference obtained using (26) and (27).

small. At higher Reynolds numbers the discrepancy is probably due to the breakdown of the asymptotic approximation (21). The effect of rotation is to increase the lift force; the rotation produces a lift that acts in the same direction as the computed lift on a non-rotating sphere. When $\sqrt{Re_G} \gg Re_s$, the rotation produces a higher order effect and its contribution can be neglected without introducing any serious errors in the estimation of the lift force. However, since the lift on a non-rotating sphere is very small in magnitude when $Re_s > Re_G^{1/2}$, the effect of rotation in such cases is comparable to the total lift force. For slip Reynolds numbers that are not large, the effect of rotation can be estimated using Saffman's second order expression (28). In this study we have not been able to investigate the lift force for small values of ϵ when the linearized momentum equations are valid (i.e. when $Re_s \ll \epsilon^2$). To achieve this condition, Re_G and Re_s would have to be very small and a very large domain would be required to obtain accurate results for the lift force. In their study, Dandy and Dwyer (1990) used a smaller domain and outflow type boundary conditions at the outer boundary. The boundary conditions are useful in reducing the size of the domain for flows in which the Oseen wake is

small and the flow outside the wake decays fast. It is not clear whether these boundary conditions can be applied to a smaller domain when the Reynolds numbers are close to unity.

Acknowledgements

This work was supported by grant DE-FG02-88ER13919 from the U.S. Department of Energy. Most of the computations were done using IBM RS6000 computers in the A.V.S. Laboratory at Clarkson University. The large domain computations were done on IBM RS6000 computers at the Cornell National Supercomputer Facility, a resource of the Cornell Theory Center, which is in part funded by the National Science Foundation, New York State, the IBM Corporation and members of the Center's Corporate Research Institute. This work was done while one of the authors, PC, was at the Chemical Engineering Department, Clarkson University, Potsdam, NY 13699.

References

Anderson, D.A., Tannehilll, J.C., Pletcher, R.H., 1984. Computational Fluid Mechanics and Heat Transfer. Hemisphere, New York.
Asmolov, E.S. 1989. Lift force exerted on a spherical particle in a laminar boundary layer. Izvestigya Akademi Nauk SSSR, Mekhanika Zhidosti i Gaza. no. 5. 66–71.
Auton, T.R., 1987. The lift force on a spherical body in a rotational flow. J. Fluid Mech. 183, 199–218.
Cherukat, P., 1993. Ph.D thesis, Clarkson University.
Cherukat, P., McLaughlin, J.B., 1993. Inertial lift on a rigid sphere in a linear shear flow field near a flat wall. J. Fluid Mech. 263, 1–18.
Cherukat, P., McLaughlin, J.B., Graham, A.L., 1994. The inertial lift on a rigid sphere translating in a linear shear flow field. Int. J. Multiphase Flow 20, 339–353.
Cox, R.G., Brenner, H., 1968. The lateral migration of solid particles in Poiseuille flow: I. Theory. Chem. Engng. Sci. 23, 147–173.
Cox, R.G., Hsu, S.K., 1977. The lateral migration of solid particles in a laminar flow near a plane. Int. J. Multiphase Flow 3, 201–222.
Cox, R.G., Mason, S.G., 1971. Suspended particles in fluid flow through tubes. Ann. Rev. Fluid Mech. 3, 291–316.
Dandy, D.S., Dwyer, H.A., 1990. A sphere in shear flow at finite Reynolds number: effect of shear on particle lift, drag and heat transfer. J. Fluid Mech. 216, 381–410.
Drew, D.A., 1988. The lift force on a small sphere in the presence of a wall. Chem. Engng. Sci. 43, 769–773.
Goldsmith, A.J., Mason, S.G., 1967. The microrheology of dispersions. Erich FR, Ed. Rheology Theory and Applications. 85–250. Academic Press, New York.
Golub, G.H., Van Loan, C.F., 1989. Matrix Computations. The Johns Hopkins University Press, Baltimore.
Ho, B.P., Leal, L.G., 1976. Inertial migration of rigid spheres in two-dimensional unidirectional flows. J. Fluid Mech. 65, 365–400.
Leighton, D.A., Acrivos, A., 1985. The lift on a small sphere touching a plane in the presence of a simple shear flow. Z. Agnew. Math. Phys. 36, 174–178.
Masliyah, J.H., Epstein, N., 1970. Numerical study of steady flow past spheroids. J. Fluid Mech. 44, 493–512.
McLaughlin, J.B., 1989. Aerosol particle deposition in numerically simulated channel flow. Phys. Fluids A1, 1211–1224.
McLaughlin, J.B., 1991. Inertial migration of a small sphere in linear shear flows. J. Fluid Mech. 224, 261–274.
McLaughlin, J.B., 1993. The lift on a small sphere in wall-bounded linear shear flows. J. Fluid. Mech. 246, 249–265.
Mei, R., 1992. An approximate expression for the shear lift force on a spherical particle at finite Reynolds number. Int. J. Multiphase Flow 18, 145–147.
Petzold, L., Lötsted, P., 1986. Numerical solution of nonlinear differential equations with algebraic constraints II: practical implications. SIAM J. Sci. Stat. Comput. 7, 720–733.
Rubinow, S.I., Keller, J.B., 1961. The transverse force on a spinning sphere moving in a viscous fluid. J. Fluid Mech. 11, 447–459.
Saad, Y., Schultz, M.H., 1986. A generalized minimal residual algorithm for solving nonsymmetric linear systems. SIAM J. Sci. Stat. Comput. 7, 856–869.
Saffman, P.G., 1965. The lift on a small sphere in a slow shear flow. J. Fluid Mech. 22, 385–400 (and Corrigendum, 31, 1968, 624).
Schonberg, J.A., Hinch, E.J., 1989. The inertial migration of a sphere in Poiseuille Flow. J. Fluid Mech. 203, 517–524.
Segré, G., Silberberg, A., 1961. Radial particle displacements in Poiseuille flow of suspensions. Nature 189, 209–210.
Vasseur, P., Cox, R.G., 1976. The lateral migration of a spherical particle in two-dimensional shear flows. J. Fluid Mech. 78, 385–413.
Vinokur, M., 1989. An analysis of finite-difference and finite-volume formulations of conservation laws. J. Comput. Phys. 81, 1–52.